FEMS Microbiology Letters, 365, 2018, fny151

doi: 10.1093/femsle/fny151
Advance Access Publication Date: 19 June 2018
Research Letter

RESEARCH LETTER – Physiology & Biochemistry

Molecular cloning, expression and biochemical characterization of periplasmic nitrate reductase from *Campylobacter jejuni*

Breeanna Mintmier[1], Jennifer M. McGarry[1], Courtney E. Sparacino-Watkins[2], Joseph Sallmen[3], Katrin Fischer-Schrader[4], Axel Magalon[5], Joseph R. McCormick[3], John F. Stolz[3], Günter Schwarz[4], Daniel J. Bain[6] and Partha Basu[1,*]

[1]Department of Chemistry and Chemical Biology, Indiana University-Purdue University, Indianapolis, IN 46202, USA, [2]Vascular Medicine Institute, University of Pittsburgh School of Medicine, PA 15213, USA, [3]Department of Biological Sciences, Duquesne University, Pittsburgh, PA 15282, USA, [4]Institute for Biochemistry, University of Cologne, Cologne 50674, Germany, [5]Aix Marseille Université, CNRS, Laboratoire de Chimie Bactérienne (UMR7283), IMM, 13402 Marseille, France and [6]Department of Geology and Environmental Science, University of Pittsburgh, PA 15260, USA

*Corresponding author: Department of Chemistry and Chemical Biology, Indiana University-Purdue University Indianapolis, 402 N Blackford St, Indianapolis, IN 46202, USA. Tel: +317 274 8935; Fax: 317 274 4701; E-mail: basup@iupui.edu

One sentence summary: Molecular cloning, expression and kinetic analysis of the native *Campylobacter jejuni* enzyme and the cysteine 176 to serine variant.

Editor: LÃgia Saraiva

ABSTRACT

Campylobacter jejuni, a human gastrointestinal pathogen, uses nitrate for growth under microaerophilic conditions using periplasmic nitrate reductase (Nap). The catalytic subunit, NapA, contains two prosthetic groups, an iron sulfur cluster and a molybdenum cofactor. Here we describe the cloning, expression, purification, and Michaelis-Menten kinetics (k_{cat} of $5.91 \pm 0.18\ s^{-1}$ and a K_M (nitrate) of $3.40 \pm 0.44\ \mu M$) in solution using methyl viologen as an electron donor. The data suggest that the high affinity of NapA for nitrate could support growth of *C. jejuni* on nitrate in the gastrointestinal tract. Site-directed mutagenesis was used and the codon for the molybdenum coordinating cysteine residue has been exchanged for serine. The resulting variant NapA is 4-fold less active than the native enzyme confirming the importance of this residue. The properties of the *C. jejuni* enzyme reported here represent the first isolation and characterization of an epsilonproteobacterial NapA. Therefore, the fundamental knowledge of Nap has been expanded.

Keywords: NapA; nitrate reductase; pathogenicity; molybdenum; *Campylobacter*; heterologous expression

Received: 19 April 2018; **Accepted:** 17 June 2018

HIGHLIGHTS

- *Campylobacter jejuni* NapA has been cloned and expressed heterologously.
- *Campylobacter jejuni* NapA has a k_{cat} of 5.91 ± 0.18 s^{-1} and a K_M (nitrate) of 3.40 ± 0.44 μM.
- A NapA-C176S variant has been isolated and has a K_M (nitrate) of 307 ± 16 μM and a k_{cat} of 0.045 ± 0.001 s^{-1}.

INTRODUCTION

Campylobacter jejuni has been classified as an emerging antibiotic-resistant pathogen worldwide (Johnson, Shank and Johnson 2017), where nearly 1% of Europe's population is infected, and the percentage is expected to be higher in developing countries (Epps *et al.* 2013). *Campylobacter jejuni* is commonly present in the gastrointestinal tract (GIT) of chickens, and can be transmitted to humans via contaminated food and/or water (Liu *et al.* 2012). In infants, *C. jejuni* infection causes severe diarrhea in 6–12% of cases and diarrhea is the second leading cause of mortality in children worldwide (Liu *et al.* 2016). *Campylobacter* infection may also be detrimental to children as it is suggested to be an important contributor to growth deficits, especially in low-resource settings (Amour *et al.* 2016). Due to the increased antibiotic resistance of *C. jejuni* and the impact on human health, specifically infants and children, physiological understanding of *C. jejuni* and development of new therapeutic strategies are crucial.

Aside from gastroenteritis infections, pathogens like *C. jejuni* have been attributed to methemoglobinemia, a disease primarily found in infants where methemoglobin is produced (Powlson *et al.* 2008). Methemoglobinemia has also been linked to well water with high concentrations of nitrate (Knobeloch *et al.* 2000). Re-evaluation of these studies indicates that the cases of incidence occurred with well water that was contaminated with feces (Powlson *et al.* 2008). Due to fecal contamination, the water contained appreciable amounts of bacterial pathogens such as *C. jejuni* as well as nitrate, implying methemoglobinemia may be induced by bacterial nitrate reduction producing NO that converts hemoglobin to methemoglobin. The nitrate reduction by *C. jejuni* has not been fully investigated despite a potential correlation between excess nitrate in well water, the presence of *C. jejuni* and methemoglobinemia. Therefore, there is a need to understand nitrate reduction in *C. jejuni* at the molecular level.

Bacterial nitrate reduction is catalyzed by a class of pterin-containing molybdenum enzymes called nitrate reductase. There are three subclasses of prokaryotic nitrate reductases: periplasmic (Nap), respiratory (Nar) and assimilatory (Nas) (Stolz and Basu 2002). Of these, *C. jejuni* only harbors the genes for Nap (Pearson *et al.* 2007). Nap is a dissimilatory enzyme complex, i.e. it is a catabolic complex that reduces nitrate. When Nap is coupled to the oxidation of formate or NADH, a proton gradient is generated enabling the production of ATP. Moreover, Nap can generate energy through nitrate respiration as part of the denitrification and dissimilatory nitrate reduction to ammonia pathways in bacteria (Stolz and Basu 2002; Sparacino-Watkins, Stolz and Basu 2014).

Unlike many pathogens, *C. jejuni* has no defining toxins and relies on other mechanisms for infection (Crofts *et al.* 2018). The key metabolic pathways, like nitrate metabolism, that boost colonization may be one such mechanism. To this end, the oxidation of various electron donors such as $FADH_2$, H_2, formate, lactate or succinate can be coupled with nitrate (NO_3^-) reduction. Succinate is readily available in the host's GIT (Hofreuter 2014) where NO_3^- reduction has been recognized as an influential factor during *C. jejuni* host colonization (Weingarten, Grimes and Olson 2008; Liu *et al.* 2012). Under inflammatory conditions the concentration of formate is increased and formate oxidation has been shown to be influenced by elevated nitrate levels (Hughes *et al.* 2017).

During colonization in chickens, *C. jejuni* induces expression of the *napAGHBLD* operon (Woodall *et al.* 2005) and during *C. jejuni* infection of mammalian cells, the expression of the catalytic subunit, NapA, is increased.(Liu *et al.* 2012) A *napA* deletion decreased the adhesion of *C. jejuni* to human INT-407 cells and impacted motility and biofilm formation (Kassem *et al.* 2012). Recently, Nap has been shown to be important in the pathogenesis of the intestinal pathogen *Salmonella typhimurium* that is also passed by poultry reservoirs to humans (Lopez *et al.* 2015). It has been demonstrated that a NapA deletion reduces the ability to infect host cells signifying Nap influences pathogenesis (Lopez *et al.* 2015). This result may indicate a common mechanism for intestinal pathogen survival via nitrate respiration using Nap.

Campylobacter jejuni NapA has not been biochemically characterized despite the significance of NO_3^- reduction by this pathogen. It has also been reported that there is a potential use of nitrate reductase genes for differentiating *Campylobacter* species (Miller *et al.* 2007). Given the paucity of biochemical characterization of *C. jejuni*, fundamental information to understand nitrate reduction by *C. jejuni* is lacking. Here we report the cloning of *napA*, heterologous expression, and biochemical characterization of recombinant NapA (from here on referred to as the native enzyme). Using the expression system we have exchanged C176 (that putatively coordinates the molybdenum center) to serine. This variant has also been purified and biochemically characterized. In addition, we also compared the kinetic results with previously isolated NapA assayed by methyl viologen in solution.

MATERIALS AND METHODS

Plasmids and oligonucleotides are listed in Table S1 (supplementary material). Chromosomal DNA from the pathogenic *C. jejuni* strain RM1221 was used as the source of *napA*, *napL* and *napD*. Polymerase chain reaction (PCR) was used to amplify *napLD* maturation genes (YP_178877 and YP_178878) and the DNA fragment was inserted into the pTZS7R/T TA cloning vector (Thermo Fisher) yielding plasmid pBM8A. The *napLD* genes were excised using NcoI and EcoRI and then inserted into the pRSFDuet-1 expression vector (Novagen) to yield plasmid pBM9A.The *napA* gene (YP_178873) was amplified using PCR and the restriction enzyme-digested fragment was inserted into the pMCSG32 vector (DNASU) using NdeI and XmaI upstream from the TEV cleavable C-terminal hexa-histidine coding sequence, yielding the pMCSG32_napA plasmid. The *napA* gene was excised with NdeI and XhoI taking the tagged gene and inserting it into the same sites of pBM9A containing the maturation genes *napLD* to yield plasmid pBM10C. Thus, pBM10C allows coexpression of his tagged *napA* with untagged *napLD* in *Escherichia coli* from separate T7 promoters. All DNA constructs were confirmed by sequencing (ACGT Inc).

Escherichia coli K12 (New England Biolabs Shuffle T7 lysY #C3027) cells containing the pBM10C plasmid were maintained on LB medium supplemented with 30 μg/mL kanamycin. Inoculated cultures were grown overnight at 37°C, then transferred

to 1 L of fresh autoinduction medium containing 12 g/L peptone, 24 g/L yeast extract, 1 g/L glucose, 2 g/L lactose, 0.50% (v/v) glycerol and 90 mM potassium phosphate buffer pH 7.00. The cultures were supplemented with kanamycin (30 μg/mL), Na_2MoO_4 (1 mM) and $FeSO_4$ (0.5 mM), then incubated at room temperature for 48 h.

NapA (104 kDa) expression was induced by the lactose present in the medium. Expression was conducted at room temperature for 48 h while shaking. Cells were collected by centrifugation at 4400 × g at 4°C. The cell pellet was resuspended in ice cold buffer containing 50 mM HEPES, 300 mM sodium chloride and 10 mM imidazole at pH 7.00. Cells were lysed by ultrasonication using 30-s pulses in 45-s intervals over 10 min in an ice bath. The lysate was centrifuged at 7100 × g for 1 h at 4°C. The soluble fraction was loaded on a HisTrap HP 5 mL prepacked column (GE Life Sciences), and separation was conducted with an ÄKTA Prime Plus (GE Life Sciences) system. The column was washed with a step gradient of 20 and 50 mM imidazole. NapA was eluted with 250 mM imidazole. The fractions were pooled and concentrated during buffer exchange to 50 mM HEPES pH 7.00 using 30 kDa cutoff centrifugal filters (Millipore). The concentrated protein was loaded onto a HiPrep 16/60 Sephacryl S-200 size exclusion column (GE Healthcare). The resulting NapA fractions were pooled, concentrated and stored in buffer containing 50 mM HEPES pH 7.00 at –80°C. SDS-PAGE was used to screen fractions for NapA content and purity using standard protocols.

Mutagenesis of *C. jejuni napA* was conducted using the QuikChange II Site-Directed Mutagenesis Kit (Qiagen) with the pBM10C plasmid as template. The primers designed for a *napA-C176S* mutation are listed in Table S1 (Supporting Information). The PCR product was sequenced at ACGT Inc. The resulting plasmid, pBM10C-C176S, was expressed in *E. coli*, and NapA-C176S was purified in the same manner as the native NapA.

Nitrate reductase activity was measured spectrophotometrically by monitoring oxidation of reduced methyl viologen at 630 nm. Methyl viologen was reduced electrochemically in an inert atmosphere glovebox using a Metrohm PGASTAT204 potentiostat in a three electrode system with an Ag/AgCl reference electrode, a platinum wire auxiliary electrode and platinum mesh as the working electrode. The potential was held at –500 mV vs SHE (midpoint potential of methyl viologen is –449 mV vs SHE at pH 7.00; Watanabe and Honda 1982) until methyl viologen was reduced. Assays were conducted in an inert atmosphere glove box at 25°C using a Bio-Tek ELx808 Absorbance Microplate Reader. Assays were conducted with a total reaction volume of 300 μL. Nitrate addition initiated the reaction which was monitored for 5 min (NapA) or 15 min (NapA-C176S). The rate of methyl viologen oxidation was calculated using the Beer-Lambert law given the extinction coefficient of reduced methyl viologen (7800 $M^{-1}cm^{-1}$ at 630 nm). These rates were analyzed with a non-linear Michaelis–Menten model using OriginPro 2018 (OriginLab Inc.). Protein concentrations were determined using the Coomassie protein assay kit (Thermo Scientific) with bovine serum albumin standard (Pierce).

RESULTS

The *napALD* genes were coexpressed resulting in the production of recombinant NapA protein with the original *C. jejuni* N-terminal twin arginine translocase (TAT) leader sequence intact to preserve the NapA chaperone interactions. The *napA* gene contained a polyhistidine tag at the C-terminus that was kept intact for this investigation. NapA-hexaHis (hereafter referred to as NapA) was isolated by immobilized metal chromatography and purified to 95% homogeneity (Fig. 1A). The identity of the purified ~100 kDa protein was confirmed to be NapA from *C. jejuni* by liquid chromatography-mass spectrometry (LC-MS).

The UV-Vis spectrum of *C. jejuni* NapA (Fig. 1C) shows a band at 400 nm similar to the band observed in the spectrum of *Desulfovibrio desulfuricans* NapA, indicating the presence of a [4Fe4S] cluster (Bursakov *et al.* 1995). The metal (Mo and Fe) content in the enzyme was determined by inductively coupled plasma mass spectrometry (ICP-MS). The metal analyses indicate 92% Mo incorporation in active *C. jejuni* NapA. The Fe:Mo ratio was slightly higher than the theoretical value of 4:1 suggesting complete iron incorporation. (Table S2, Supporting Information)

Campylobacter jejuni NapA displays Michaelis-Menten kinetics (Fig. 2), with a calculated maximum velocity (V_{max}) of 3.40 ± 0.10 μmoles min^{-1} mg $protein^{-1}$ and a K_M for NO_3^- of 3.40 ± 0.44 μM. We determined a k_{cat} of 5.91 ± 0.18 s^{-1} and calculated a kinetic putative second order rate (k_{cat}/K_M) constant of 1.74 × 10^6 M^{-1} s^{-1}. A comparison of the K_M and V_{max} values with those reported for other characterized NapA (Table 1) reveals important differences in the kinetic properties. The major difference is the low K_M of the heterologously produced *C. jejuni* NapA which indicates a high binding affinity for NO_3^-.

A three-dimensional model of the *C. jejuni* NapA structure was created using the structure of *Rhodobacter sphaeroides* NapA as the template (Sparacino-Watkins, Stolz and Basu 2014). The electrostatic potential was calculated for *C. jejuni* NapA, and, for comparison, the *R. sphaeroides*, *D. desulfuricans* and *E. coli* NapA structures (Fig. 3). In all structures, a dense region of positive charge is localized in the active site funnel, possibly used to facilitate the transport of NO_3^- into the cavity for catalytic transformation. The homology model (Sparacino-Watkins, Stolz and Basu 2014) suggests the substrate channel and catalytic pocket are more basic than other NapA proteins, which may influence the substrate binding as well as product release.

Based on the homology model of *C. jejuni* NapA and the protein sequence alignment (Fig. S1, Supporting Information), we predicted that a strictly conserved cysteine at position 176 (C176), modeled in Fig. 3 (Sparacino-Watkins, Stolz and Basu 2014), is likely to coordinate the molybdenum center in *C. jejuni*. We hypothesize that a C176S mutation would reduce the catalytic activity of the enzyme. Similar mutations have been reported for related molybdenum enzymes including sulfite oxidase (coordinating Cys to Ser/Ala), biotin sulfoxide reductase (coordinating Ser to Cys/Ala/Thr), DMSO reductase (coordinating Ser to Cys/Ala/His), Nas (coordinating Cys to Ala) and Nap (coordinating Cys to Ser) (Garde, Kinghorn and Tomsett 1995; Garrett and Rajagopalan 1996; Trieber *et al.* 1996; Hilton, Temple and Rajagopalan 1999; Pollock and Barber 2000; Hettmann *et al.* 2004; Qiu *et al.* 2010). These variants reduced or completely abolished activity compared to the native enzyme but there are no reports of determined rate constants (k_{cat} or K_M) (Table 2).

The NapA-C176S variant was observed to be pure to 97% homogeneity via SDS-PAGE (Fig. 1B). The identity of NapA and the presence of C176S substitution were confirmed by LC-MS (Fig. S2, Supporting Information) and metal content was determined by ICP-MS (Table S2, Supporting Information). Kinetic experiments with NapA-C176S indicated that this variant was active in reducing NO_3^- as a substrate but had significantly lower activity when compared to the native enzyme (Fig. 2). This mutation increased the K_M (307 ± 16 μM) and reduced the k_{cat} (0.045 ± 0.001 s^{-1}) by two orders of magnitude.

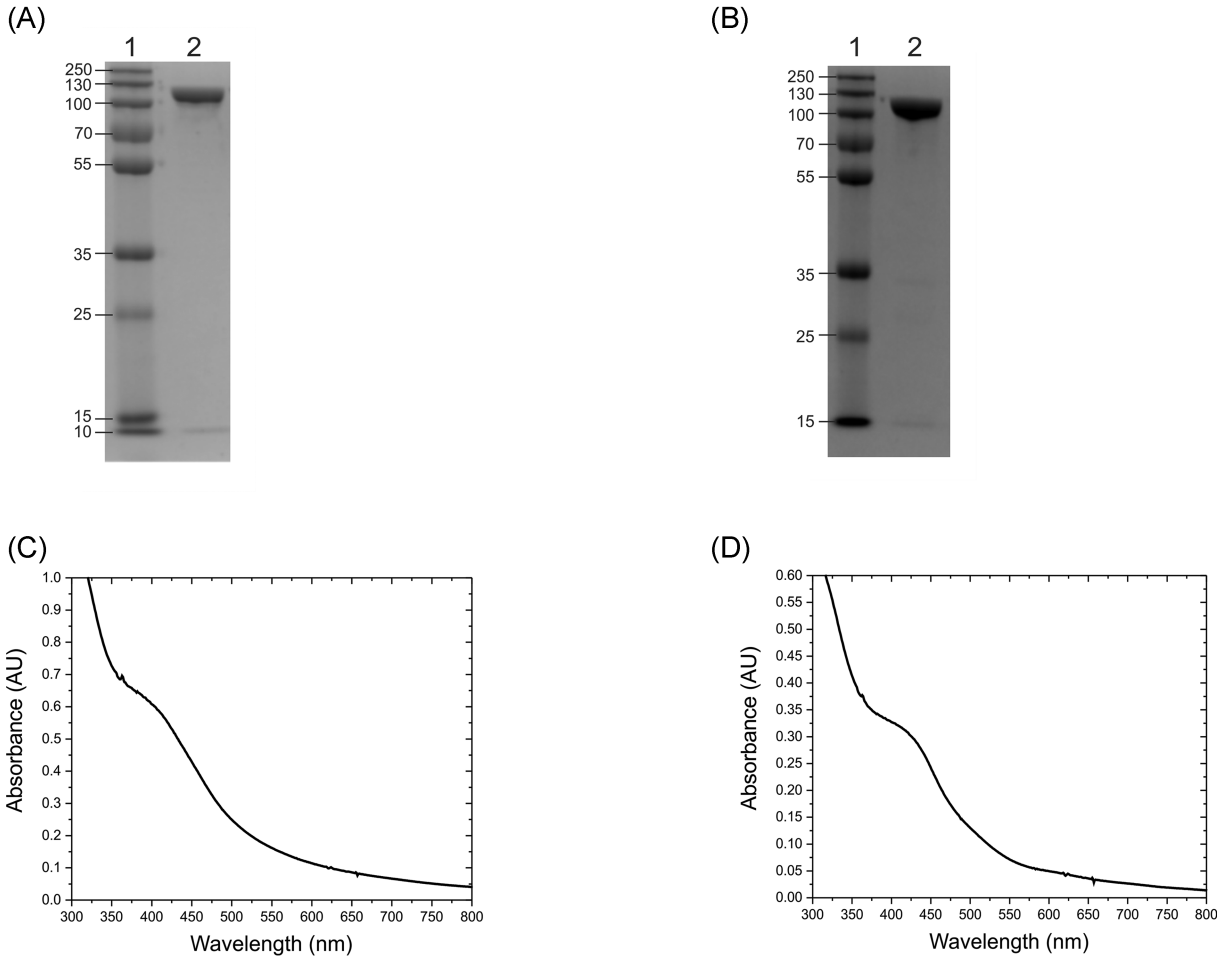

Figure 1. Characterization of native and variant *C. jejuni* NapA by gel electrophoresis and UV-vis spectroscopy. (**A**) SDS PAGE image of the NapA, (**B**) SDS PAGE image of the NapA-C176S variant where lane 1 is the molecular weight standards in kDa, (**C**) UV-vis spectrum of the as-prepared recombinant NapA in 50 mM HEPES pH 7.00, (**D**) UV-Vis spectrum of the as-prepared NapA-C176S variant in 50 mM HEPES pH 7.00.

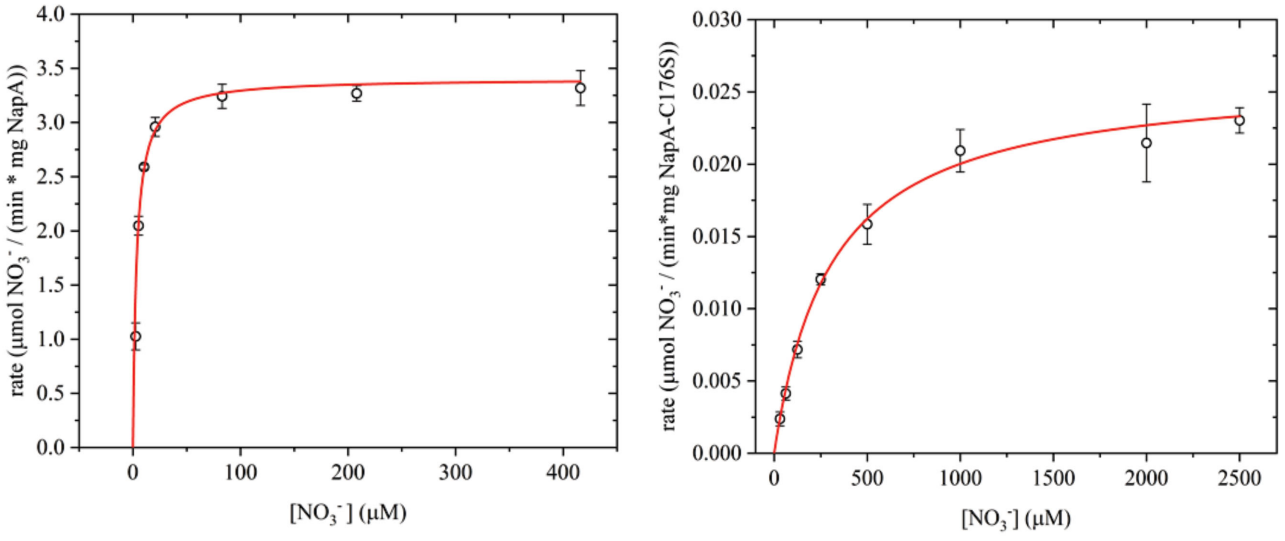

Figure 2. Steady-state kinetic analysis using the Michaelis-Menten model. Left panel: steady-state kinetics of the reduction of nitrate by *C. jejuni* NapA. Right panel: steady-state kinetics of the reduction of nitrate by *C. jejuni* NapA-C176S variant. Note the Y-axes are different by ~2 orders of magnitude and the solid lines represent Michaelis-Menten fit.

Table 1. Kinetic parameters reported for NapA (A) or NapAB (AB) in various organisms using the methyl/benzyl viologen solution assay.

Organism	pH	K_M (μM)	k_{cat} (s^{-1})	V_{max} (μmoles nitrate min^{-1} mg^{-1})	k_{cat}/K_M (M^{-1} s^{-1})	Reference
Campylobacter jejuni (A)	7.00	3.40 ± 0.44	5.91 ± 0.18	3.40 ± 0.10	1.74×10^6	This work
Rhodobacter sphaeroides (A)	7.00	120.00	70.20[a]	39.00	5.85×10^5	Sabaty *et al.* (2001)
Paracoccus pantotrophus (AB)	7.00	112.00	58.00		5.18×10^5	Gates, Richardson and Butt (2008)
Paracoccus pantotrophus (AB)	7.20	1300.00	240.00		1.85×10^5	Butler *et al.* (1999)
Magnetospirillum magnetotacticum (AB)	7.00	3.20	2.50		7.81×10^5	Taoka *et al.* (2003)
Aliivibrio fischeri (AB)	7.50	65.00	10.00[a]	1.50	1.54×10^5	Sadana and McElroy (1957)

[a]Values calculated from kinetic parameters using the reported protein concentrations.

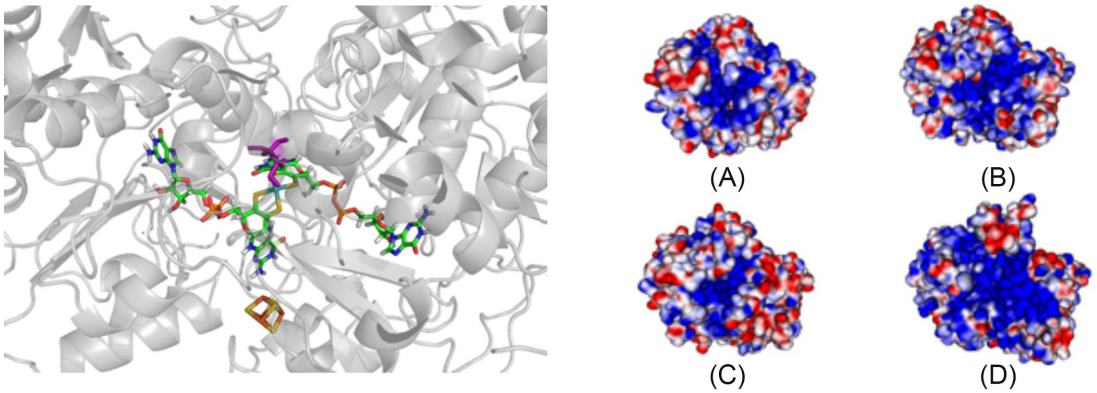

Figure 3. Calculated structure and electrostatic potential map of NapA. Left panel: Pymol rendering of the metal centers of *C. jejuni* NapA homology model depicting the target for mutation, residue C176 (purple). Moco and the [4Fe4S] cluster are colored by element. The protein backbone is in gray. Right panel: the electrostatic potential plots for NapA showing the active site face of (a) *D. desulfuricans*, (b) *E. coli*, (c) *R. sphaeroides* and (d) *C. jejuni*. *Desulfovibrio desulfuricans*, *E. coli* and *R. sphaeroides* structure data were downloaded from PBD.org database. Comparison of the electrostatic maps reveals that NapA from *C. jejuni* is the most basic, as indicated by the blue color, while *R. sphaeroides* is the most acidic (red). *Desulfovibrio desulfuricans* and *E. coli* electrostatic potential maps are intermediate. The NapA structures were aligned and the electrostatic potentials were calculated in Pymol (–10 kT = red; 10 kT = blue; 0 kT = white).

Table 2. Reported mutations of the molybdenum coordinating residue in various mononuclear molybdenum enzymes.

Enzyme	Mutation	Activity (% of WT)	Reference
C. jejuni NapA	C176S	0.78%	This work
Chicken SO	C185S	Inactive	Qiu *et al.* (2010)
Chicken SO	C185A	Inactive	Qiu *et al.* (2010)
Human SO	C207S	<<1.00%	Garrett and Rajagopalan (1996)
R. sphaeroides BSOR	S121A	0.30–3.00%[a]	Pollock and Barber (2000)
R. sphaeroides BSOR	S121T	0.30–3.00%[a]	Pollock and Barber (2000)
R. sphaeroides BSOR	S121C	0.30–3.00%[a]	Pollock and Barber (2000)
R. sphaeroides DMSOR	S147C	37.00–41.00%	Hilton, Temple and Rajagopalan (1999)
E. coli DMSOR	S176A	<4.00%[a]	Trieber *et al.* (1996)
E. coli DMSOR	S176C	<4.00%[a]	Trieber *et al.* (1996)
E. coli DMSOR	S176H	<4.00%[a]	Trieber *et al.* (1996)
Aspergillus nidulans Nas	C150A	Inactive	Garde, Kinghorn and Tomsett (1995)
Cupriavidus necator Nap	C181S	Inactive	Hettmann *et al.* (2004)

[a]Activity is indistinguishable from background, calculated from reported specific activity.
SO, sulfite oxidase; DMSOR, dimethyl sulfoxide reductase; BSOR, biotin sulfoxide reductase; Nas, assimilatory nitrate reductase; Nap, periplasmic nitrate reductase.

DISCUSSION

NapA has been isolated from native organisms as a heterodimer with the diheme *c*-type cytochrome NapB, from *E. coli* (Jepson *et al.* 2007), *R. sphaeroides* (Arnoux *et al.* 2003), *Achromobacter fischeri* (Sadana and McElroy 1957), *Cupriavidus necator* (Coelho *et al.* 2007) and *Thiosphaera pantotropha* (Berks *et al.* 1994), or as a monomer from *D. desulfuricans* (Bursakov *et al.* 1995). Whether the Nap is monomeric or heterodimeric depends on its ability to form salt bridges at the NapA:NapB interface (Simpson, McKinzie and Codd 2010). Two residues E76 and S801 (in *R. sphaeroides*, *Rs*; Fig. S1, Supporting Information) have been identified as critical for the formation of the NapAB heterodimer (Simpson, McKinzie and Codd 2010). The sequence alignment of *C. jejuni* NapA with *R. sphaeroides* NapA shows the presence of a proline (P70) instead of a critical

glutamate precluding the formation of the salt bridge, and thus *C. jejuni* NapA was expected to be a monomer in solution. *Escherichia coli* NapA also contains this proline substitution, and Jepson *et al.* (2007) reported that although NapA and NapB interact, the NapAB complex is not tight and the subunits purify independently. NapA representatives from each class of gram-negative Proteobacteria have been isolated except the Epsilonproteobacteria. The class of Epsilonproteobacteria includes notable human pathogens like *Helicobacter* and *Campylobacter* species. To date, this is the first active epsilonproteobacterial NapA to be isolated and have its enzymatic properties explored.

Successful heterologous production of a metalloprotein often requires the coexpression of genes encoding dedicated chaperones to ensure proper folding and metal center insertion. Expression of *Pseudomonas* strain G-179 NapA in *E. coli*, without the cognate maturation proteins, resulted in non-functional NapA found in inclusion bodies (Bedzyk, Wang and Ye 1999). Genetic experiments with *Wolinella succinogenes* show *napL* and *napD* to be critical for full activity in a similar Nap system (Kern, Mager and Simon 2007). These studies emphasize the importance of maturation proteins in obtaining functional enzyme. To maximize heterologous production of active NapA containing both a molybdenum cofactor and a [4Fe4S] cluster, the maturation proteins NapL and NapD were coexpressed in this study. In addition, the TAT leader sequence on NapA was not modified to preserve the possible interactions with these maturation proteins. The *C. jejuni* TAT sequence varies from the *E. coli* sequence (Fig. S1, Supporting Information); however, pure active enzyme was isolated despite this difference. The UV-Vis spectrum (Fig. 1C) is indicative of the iron-sulfur cluster, which is supported by the ICP-MS data. Furthermore, the high molybdenum incorporation confirms an effective expression system for active *C. jejuni* NapA has been achieved. To our knowledge, this represents the first example of a heterologously expressed functional periplasmic nitrate reductase.

The data presented here reveal that *C. jejuni* NapA is a very efficient NO_3^- reducing enzyme with a high k_{cat}/K_M value and low K_M. The low K_M indicates a high binding affinity for NO_3^- (Table 1), which is consistent with the electrostatic potential calculations (Fig. 3) (Sparacino-Watkins, Stolz and Basu 2014). The low K_M could prove useful to the pathogen when competing for nitrate with the commensal nitrate utilizing organisms of the host microflora. Nitrate metabolism has been positively associated with colonization by *Salmonella* (Lopez *et al.* 2015), *E. coli* (Winter *et al.* 2013) and *C. jejuni* (Kassem *et al.* 2012).

Both solution-based assay and protein film voltammetry (PFV) have been used in understanding the kinetic properties of Nap, although they exhibit some differences. For example, *R. sphaeroides* NapAB has a reported K_M of 7.50 μM, which is comparable to the *C. jejuni* NapA K_M of 3.40 μM (Frangioni *et al.* 2004). Interestingly, Bertrand *et al.* (2007) argued the K_M measured in solution assays potentially depends on all rates in the catalytic cycle and will depart from K_M determined by PFV, if intermolecular electron transfer is the rate determining step in solution assays. The K_M values determined in solution may be higher than those determined by PFV. For this reason, we only discuss solution-based parameters obtained by using reduced methyl viologen as an electron donor (Table 1).

Compared to other Nap proteins in Table 1, *C. jejuni* NapA has the second highest substrate affinity, second only to *Magnetospirillum magnetotacticum*. Interestingly, *M. magnetotacticum* prefers microaerobic environments like *C. jejuni* (Maratea and Blakemore 1981). Although *M. magnetotacticum* is not known to be pathogenic, its *nap* operon does appear to be phylogenetically closer to *C. jejuni nap* than its fellow α-proteobacteria (Sparacino-Watkins, Stolz and Basu 2014). Furthermore, *C. jejuni* NapA appears to be a more efficient NO_3^- reducer than NapA from *M. magnetotacticum* as well as all other reported Nap proteins (Table 1) by approximately one order of magnitude in the k_{cat}/K_M. Although the k_{cat}/K_M is higher, k_{cat} itself is lower than the homologously expressed Naps in Table 1. A lower k_{cat} may be attributable to substrate/product inhibition, attenuated electron transfer or conformational change. However, the exact reason for a lower k_{cat} remains an open question.

Campylobacter jejuni NapA is expected to and does exhibit a higher affinity towards NO_3^-. We suggest there is a higher affinity for NO_3^- by *C. jejuni* NapA because it encounters low concentrations of NO_3^- under physiological conditions (Winter *et al.* 2013; Lopez *et al.* 2015). Although the inflammatory response increases nitrate concentration in the GIT of the host (Winter *et al.* 2013; Lopez *et al.* 2015; Hughes *et al.* 2017), the concentration is below 1 mM (Winter *et al.* 2013; Lopez *et al.* 2015). Nap is expressed maximally at 1 mM and does not express above 6 mM while Nar expresses maximally at 10 mM and does not express below 1 mM suggesting that Nap will be the primary nitrate reductase expressed at a low nitrate concentration (Wang, Tseng and Gunsalus 1999). Therefore, a pathogen that uses Nap may have an advantage under these conditions and Nap may exhibit a high affinity for NO_3^- (Lopez *et al.* 2015).

It has been suggested that Nap faces the periplasm and acts as a NO_3^- scavenger as Nap does not depend on NO_3^- transport (Simpson, Richardson and Codd 2010). It is interesting that *C. jejuni* NapA has a higher binding affinity for NO_3^- (low K_M) and a higher efficiency for producing nitrite than the NapA proteins from the non-pathogenic microbes. Genetic experimentation suggests that NO_3^- metabolism is important in the physiology of *C. jejuni* (Woodall *et al.* 2005; Kassem *et al.* 2012; Liu *et al.* 2012). The high efficiency of this enzyme compared to Nap proteins from non-pathogenic organisms suggests nitrate metabolism is important to this intestinal pathogen, but its role in pathogenicity is not completely clear. We suggest that NO_3^- is one of the metabolites or substrates that the pathogen relies on to ensure proper colonization into the gut of its host.

We have successfully altered the Mo coordinating residue in NapA, cysteine 176, to serine (Fig. S2, Supporting Information). The resulting variant is analogous to the coordination of Mo in DMSO reductase and trimethylamine N-oxide reductase (Li *et al.* 2000). Similar alterations in other Mo enzymes show negligible or no activity (Table 2). In these cases, steady-state kinetic parameters, K_M and $k_{cat,}$ were not reported. We have conducted Michaelis Menten kinetics on the *C. jejuni* NapA-C176S variant. This variant can reduce nitrate; however, the efficiency is lowered by four orders of magnitude. Interestingly, the K_M changed by two orders of magnitude suggesting the serine residue impacts substrate affinity as well. We suggest that the mutation could induce a rearrangement of the active site altering substrate access or by destabilizing a key interaction that assists in substrate docking. The overall reduction in the catalytic rate is also modulated by this mutation, possibly in part due to a change in redox potential of the Mo center. Such a change in the reduction potential has been observed in model complexes (Uhrhammer and Schultz 2004).

In summary, *C. jejuni* NapA has been heterologously expressed in *E. coli*. To our knowledge, this is the first example of a functional NapA from an epsilonproteobacterium that has been overexpressed and purified. Kinetic analysis of *C. jejuni* NapA revealed a high substrate binding affinity and kinetic efficiency. The sequence alignment of NapA suggests C176 coordinates Mo.

When this residue is exchanged for a serine, NO_3^- reductase activity is severely attenuated. The high substrate affinity (low μM range) of *C. jejuni* NapA suggests the Nap system has a role in scavenging for NO_3^- which has a relatively low concentration in the GIT with NO_3^- concentrations under 1 mM. Even during inflammation when nitric oxide synthase is overexpressed leading to a higher production of nitrate, the nitrate concentration does not exceed 1 mM (Winter *et al.* 2013; Lopez *et al.* 2015). These findings are in agreement with Lopez *et al.* and underscore the importance of Nap in the physiology of pathogens such as *C. jejuni*.

SUPPLEMENTARY DATA

Supplementary data are available at *FEMSLE* online.

ACKNOWLEDGEMENTS

We thank Drs A. Andrew Pacheco for discussions, and Lina Bird and Peter Chovanec for preliminary experiments. We thank Dr William Miller for genomic DNA of *C. jejuni* RM1221. We greatly appreciate all assistance from Dr Maissa Gaye for preliminary LC-MS experiments and Dr Gabriel Filippelli for preliminary ICP-OES experiments. Partial support of this work from PA CURE, DOE (DE-FG027ER64372) and National Institute of Health (GM061555 to PB) is gratefully acknowledged.

AUTHOR CONTRIBUTIONS

CSW conducted preliminary NapA experiments in various expression systems. KFS, GS, AM, JS, JRM aided in the molecular cloning aspects. JFS made intellectual contributions in biochemical aspects. DJB provided expertise and assistance with ICP-MS. JMM conducted native NapA kinetics and LC-MS confirmation of protein isolates. BM conducted bioinformatic analyses, molecular cloning, protein isolation, mutagenesis experiments, and NapA-C176S kinetics. BM and PB wrote the majority of the manuscript while all authors contributed to the editing.

Conflict of interest. None declared.

REFERENCES

Amour C, Mduma E, Gratz J *et al.* Epidemiology and impact of campylobacter infection in children in 8 Low-Resource settings: Results from the MAL-ED Study. *Clin Infect Dis* 2016;**63**:1171–9.

Arnoux P, Sabaty M, Alric J *et al.* Structural and redox plasticity in the heterodimeric periplasmic nitrate reductase. *Nat Struct Mol Biol* 2003;**10**:928–34.

Bedzyk L, Wang T, Ye RW. The periplasmic nitrate reductase in *Pseudomonas* sp. strain G-179 catalyzes the first step of denitrification. *J Bacteriol* 1999;**181**:2802–6.

Berks BC, Richardson DJ, Robinson C *et al.* Purification and characterization of the periplasmic nitrate reductase from *Thiosphaera pantotropha*. *Eur J Biochem* 1994;**220**:117–24.

Bertrand P, Frangioni B, Dementin S *et al.* Effects of slow substrate binding and release in redox enzymes: theory and application to periplasmic nitrate reductase. *J Phys Chem B* 2007;**111**:10300–11.

Bursakov S, Liu M-Y, Payne WJ *et al.* Isolation and preliminary characterization of a soluble nitrate reductase from the sulfate reducing organism *Desulfovibrio desulfuricans* ATCC 27774. *Anaerobe* 1995;**1**:55–60.

Butler CS, Charnock JM, Bennett B *et al.* Models for molybdenum coordination during the catalytic cycle of periplasmic nitrate reductase from *Paracoccus denitrificans* derived from EPR and EXAFS spectroscopy. *Biochemistry* 1999;**38**:9000–12.

Coelho C, González PJ, Trincão J *et al.* Heterodimeric nitrate reductase (NapAB) from *Cupriavidus necator* H16: purification, crystallization and preliminary X-ray analysis. *Acta Crystallogr F* 2007;**63**:516–9.

Crofts AA, Poly FM, Ewing CP *et al.* *Campylobacter jejuni* transcriptional and genetic adaptation during human infection. *Nat Microbiol* 2018;**3**:494–502.

Epps SVR, Harvey RB, Hume ME *et al.* Foodborne *Campylobacter*: infections, metabolism, pathogenesis and reservoirs. *Int J Environ Res Pu* 2013;**10**:6292–304, 6213 pp.

Frangioni B, Arnoux P, Sabaty M *et al.* In *Rhodobacter sphaeroides* respiratory nitrate reductase, the kinetics of substrate binding favors intramolecular electron transfer. *J Am Chem Soc* 2004;**126**:1328–9.

Garde J, Kinghorn JR, Tomsett AB. Site-directed mutagenesis of nitrate reductase from *Aspergillus nidulans*. Identification of some essential and some nonessential amino acids among conserved residues. *J Biol Chem* 1995;**270**:6644–50.

Garrett RM, Rajagopalan KV. Site-directed mutagenesis of recombinant sulfite oxidase. *J Biol Chem* 1996;**271**:7387–91.

Gates AJ, Richardson DJ, Butt JN. Voltammetric characterization of the aerobic energy-dissipating nitrate reductase of *Paracoccus pantotrophus*: exploring the activity of a redox-balancing enzyme as a function of electrochemical potential. *Biochem J* 2008;**409**:159–68.

Hettmann T, Siddiqui RA, Frey C *et al.* Mutagenesis study on amino acids around the molybdenum centre of the periplasmic nitrate reductase from *Ralstonia eutropha*. *Biochem Bioph Res Co* 2004;**320**:1211–9.

Hilton JC, Temple CA, Rajagopalan KV. Re-design of *Rhodobacter sphaeroides* dimethyl sulfoxide reductase. Enhancement of adenosine N1-oxide reductase activity. *J Biol Chem* 1999;**274**:8428–36.

Hofreuter D. Defining the metabolic requirements for the growth and colonization capacity of *Campylobacter jejuni*. *Front Cell Infect Microbiol* 2014;**4**:137.

Hughes ER, Winter MG, Duerkop BA *et al.* Microbial respiration and formate oxidation as metabolic signatures of inflammation-associated dysbiosis. *Cell Host Microbe* 2017;**21**:208–19.

Jepson BJN, Mohan S, Clarke TA *et al.* Spectropotentiometric and structural analysis of the periplasmic nitrate reductase from *Escherichia coli*. *J Biol Chem* 2007;**282**:6425–37.

Johnson TJ, Shank JM, Johnson JG. Current and potential treatments for reducing campylobacter colonization in animal hosts and disease in humans. *Front Microbiol* 2017;**8**:487.

Kassem II, Khatri M, Esseili MA *et al.* Respiratory proteins contribute differentially to *Campylobacter jejuni*'s survival and in vitro interaction with host's intestinal cells. *BMC Microbiol* 2012;**12**:258.

Kern M, Mager AM, Simon J. Role of individual *nap* gene cluster products in NapC-independent nitrate respiration of *Wolinella succinogenes*. *Microbiology* 2007;**153**:3739–47.

Knobeloch L, Salna B, Hogan A *et al.* Blue babies and nitrate-contaminated well water. *Environ Health Perspect* 2000;**108**:675–8.

Li H-K, Temple C, Rajagopalan KV *et al.* The 1.3 Å crystal structure of *Rhodobacter sphaeroides* dimethyl sulfoxide reductase reveals two distinct molybdenum coordination environments. *J Am Chem Soc* 2000;**122**:7673–80.

Liu J, Platts-Mills JA, Juma J *et al*. Use of quantitative molecular diagnostic methods to identify causes of diarrhoea in children: a reanalysis of the GEMS case-control study. *Lancet North Am Ed* 2016;**388**:1291–301.

Liu X, Gao B, Novik V *et al*. Quantitative proteomics of intracellular *Campylobacter jejuni* reveals metabolic reprogramming. *PLoS Pathog* 2012;**8**:e1002562.

Lopez CA, Rivera-Chavez F, Byndloss MX *et al*. The periplasmic nitrate reductase napABC supports luminal growth of *Salmonella enterica* serovar typhimurium during colitis. *Infect Immun* 2015;**83**:3470–8.

Maratea D, Blakemore RP. Aquaspirillium magnetotactium sp. nov, a Magnetic Spirillum. *Int J Syst Evol Microbiol* 1981;**31**:452–5.

Miller WG, Parker CT, Heath S *et al*. Identification of genomic differences between *Campylobacter jejuni* subsp. jejuni and *C. jejuni* subsp. doylei at the nap locus leads to the development of a *C. jejuni* subspeciation multiplex PCR method. *BMC Microbiol* 2007;**7**:11.

Pearson BM, Gaskin DJH, Segers RPAM *et al*. The complete genome sequence of *Campylobacter jejuni* strain 81116 (NCTC11828). *J Bacteriol* 2007;**189**:8402–3.

Pollock VV, Barber MJ. Serine 121 is an essential amino acid for biotin sulfoxide reductase functionality. *J Biol Chem* 2000;**275**:35086–90.

Powlson DS, Addiscott TM, Benjamin N *et al*. When does nitrate become a risk for humans? *J Environ Qual* 2008;**37**:291–5.

Qiu JA, Wilson HL, Pushie MJ *et al*. The structures of the C185S and C185A mutants of sulfite oxidase reveal rearrangement of the active site. *Biochemistry* 2010;**49**:3989–4000.

Sabaty M, Avazeri C, Pignol D *et al*. Characterization of the reduction of selenate and tellurite by nitrate reductases. *Appl Environ Microb* 2001;**67**:5122–6.

Sadana JC, McElroy WD. Nitrate reductase from *Achromobacter fischeri*. purification and properties: function of flavines and cytochrome. *Arch Biochem Biophys* 1957;**67**:16–34.

Simpson PJL, McKinzie AA, Codd R. Resolution of two native monomeric 90kDa nitrate reductase active proteins from *Shewanella gelidimarina* and the sequence of two napA genes. *Biochem Bioph Res Co* 2010;**398**:13–18.

Simpson PJL, Richardson DJ, Codd R. The periplasmic nitrate reductase in Shewanella: the resolution, distribution and functional implications of two NAP isoforms, NapEDABC and NapDAGHB. *Microbiology* 2010;**156**:302–12.

Sparacino-Watkins C, Stolz JF, Basu P. Nitrate and periplasmic nitrate reductases. *Chem Soc Rev* 2014;**43**:676–706.

Stolz JF, Basu P. Evolution of nitrate reductase: molecular and structural variations on a common function. *ChemBioChem* 2002;**3**:198–206.

Taoka A, Yoshimatsu K, Kanemori M *et al*. Nitrate reductase from the magnetotactic bacterium *Magnetospirillum magnetotacticum* MS-1: Purification and sequence analyses. *Can J Microbiol* 2003;**49**:197–206.

Trieber CA, Rothery RA, Weiner JH. Consequences of removal of a molybdenum ligand (DmsA-Ser-176) of *Escherichia coli* dimethyl sulfoxide reductase. *J Biol Chem* 1996;**271**:27339–45.

Uhrhammer D, Schultz FA. Modulation of molybdenum-centered redox potentials and electron-transfer rates by sulfur versus oxygen ligation. *Inorg Chem* 2004;**43**:7389–95.

Wang H, Tseng C-P, Gunsalus RP. The napF and narG nitrate reductase operons in *Escherichia coli* are differentially expressed in response to submicromolar concentrations of nitrate but not nitrite. *J Bacteriol* 1999;**181**:5303–8.

Watanabe T, Honda K. Measurement of the extinction coefficient of the methyl viologen cation radical and the efficiency of its formation by semiconductor photocatalysis. *J Phys Chem* 1982;**86**:2617–9.

Weingarten RA, Grimes JL, Olson JW. Role of *Campylobacter jejuni* respiratory oxidases and reductases in host colonization. *Appl Environ Microbiol* 2008;**74**:1367–75.

Winter SE, Winter MG, Xavier MN *et al*. Host-derived nitrate boosts growth of *E. coli* in the inflamed gut. *Science* 2013;**339**:708–11.

Woodall CA, Jones MA, Barrow PA *et al*. *Campylobacter jejuni* gene expression in the chick cecum: Evidence for adaptation to a low-oxygen environment. *Infect Immun* 2005;**73**:5278–85.